Electronic Supplementary Material (ESI) for CrystEngComm.
This journal is © The Royal Society of Chemistry 2021

Supporting Information

Polymorphs and Hydrates of an Anticancer Drug Erlotinib: X-ray Crystallography, Phase Transition and Biopharmaceutical Studies

Shridhar H. Thorat,[a,c] Christy P. George,[a,c] Parth S. Shaligram,[a] Suresha P. R.,[b] and Rajesh G Gonnade[*a,c]*

[a]Physical and Materials Chemistry Division, CSIR-National Chemical Laboratory, Dr. Homi Bhabha Road, Pashan, Pune, India.

[b]Polymer Science and Engineering Division, CSIR-National Chemical Laboratory, Dr. Homi Bhabha Road, Pashan, Pune, India.

[c]Academy of Scientific and Innovative Research (AcSIR), Sector 19, Kamla Nehru Nagar, Ghaziabad, Uttar Pradesh 201002, India.

E-mail: rg.gonnade@ncl.res.in; Fax: +91 20 25902642; Tel: +91 20 25902225

Table of contents

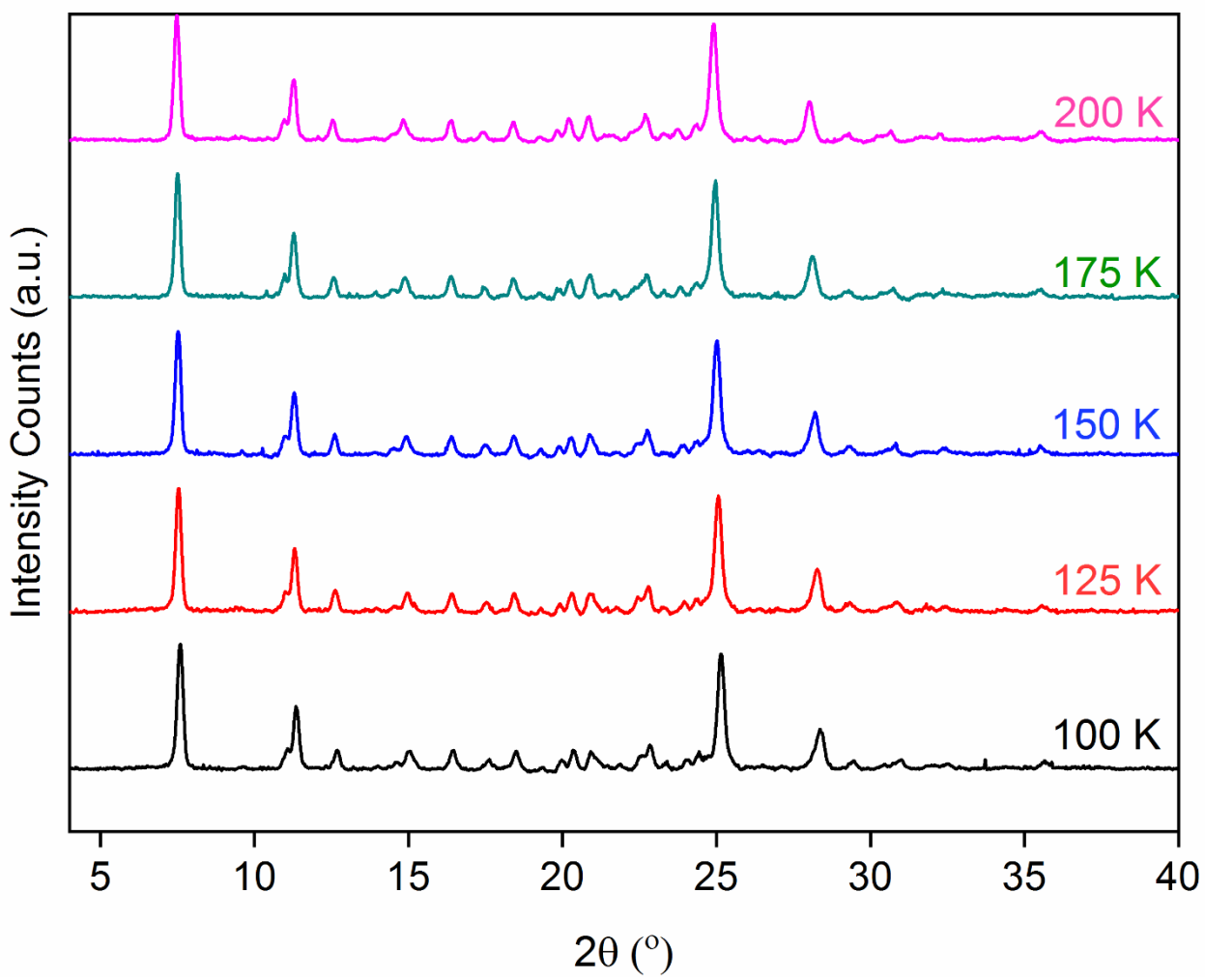

Figure S1. The variable temperature powder X-ray diffraction profile of Form I (monohydrate) of erlotinib.

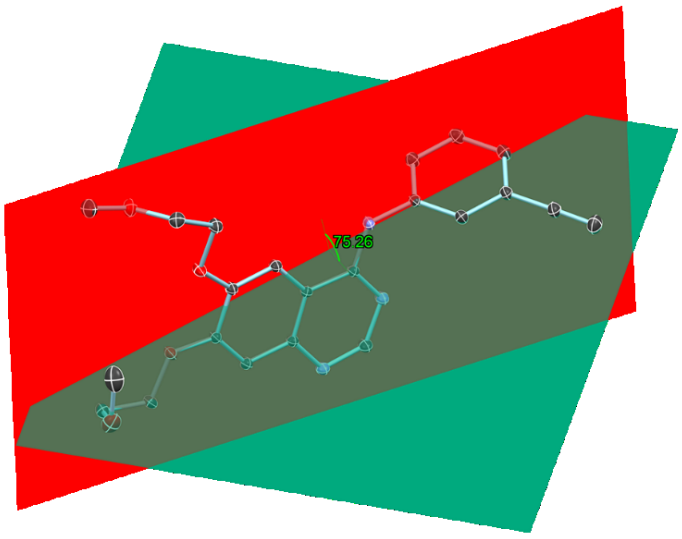

(a)

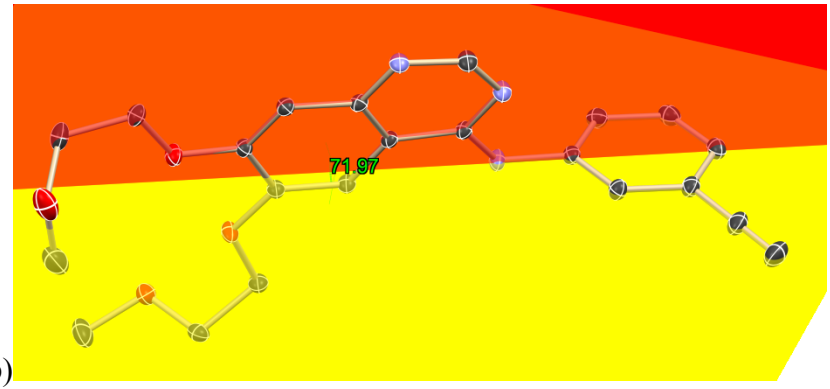

(b)

Figure S2. The conformational difference between planar moieties, quinazoline, and ethynylbenzene in (a) unprimed and (b) primed molecules of Form I crystals.

(a)

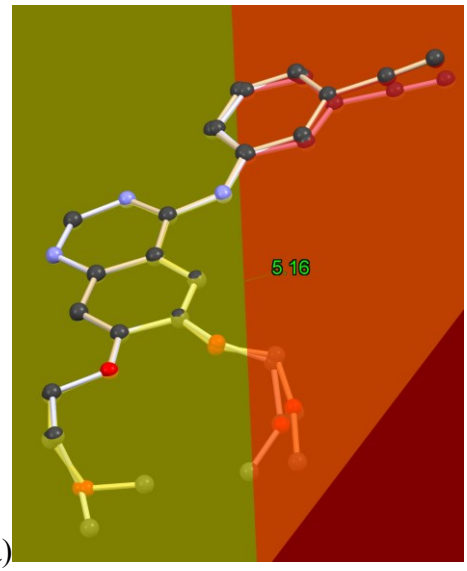

(b)

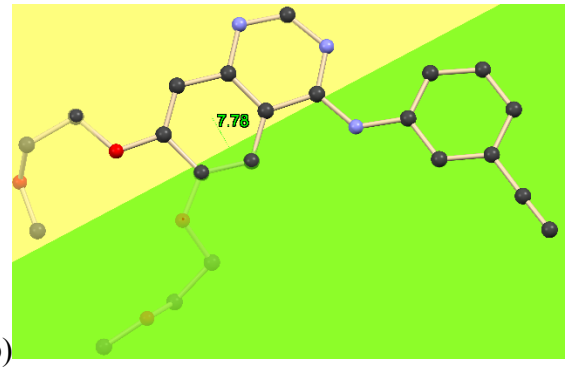

(c)

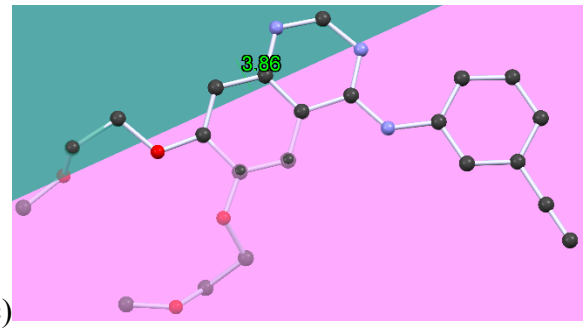

Figure S3. (a) The conformational difference between ethynylbenzene moieties of both unprimed and primed molecules, (b, c) the orientation variation between planar moieties, quinazoline, and ethynylbenzene in unprimed and primed molecules, respectively, in Form III crystals.

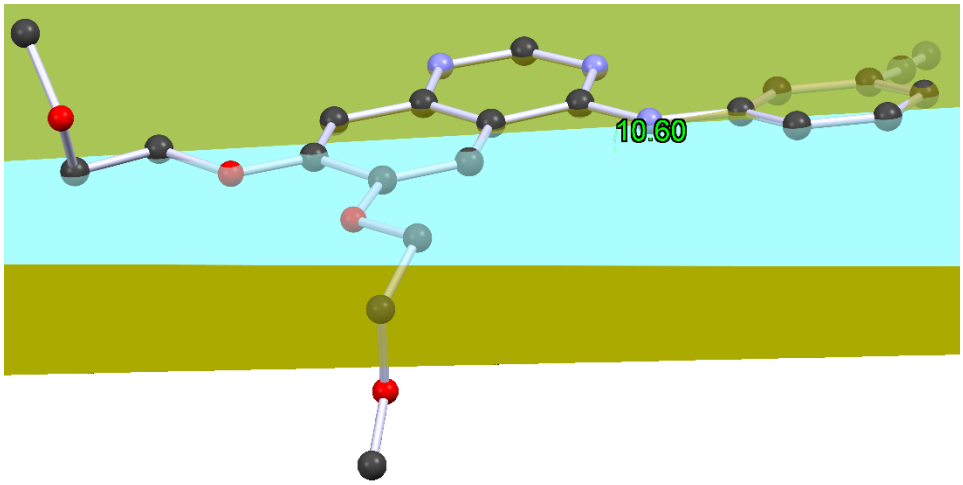

Figure S4. The conformational difference between both planar moieties, quinazoline, and ethynylbenzene in Form IV crystals.

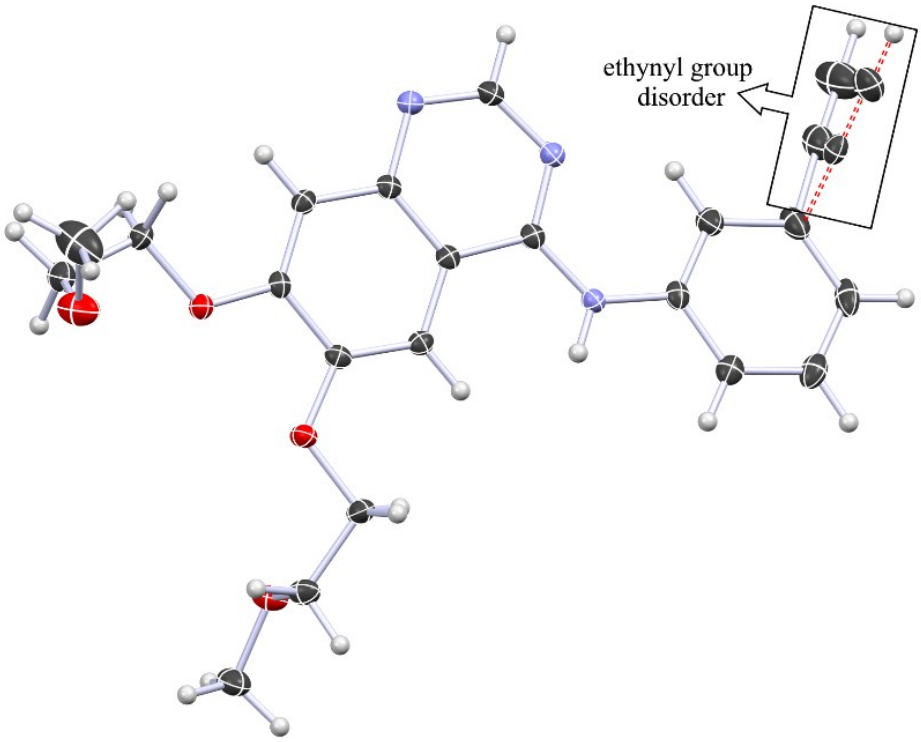

Figure S5. ORTEP of Form IV crystal displaying the ethynyl group positional disorder over two positions with equal occupancies (50%).

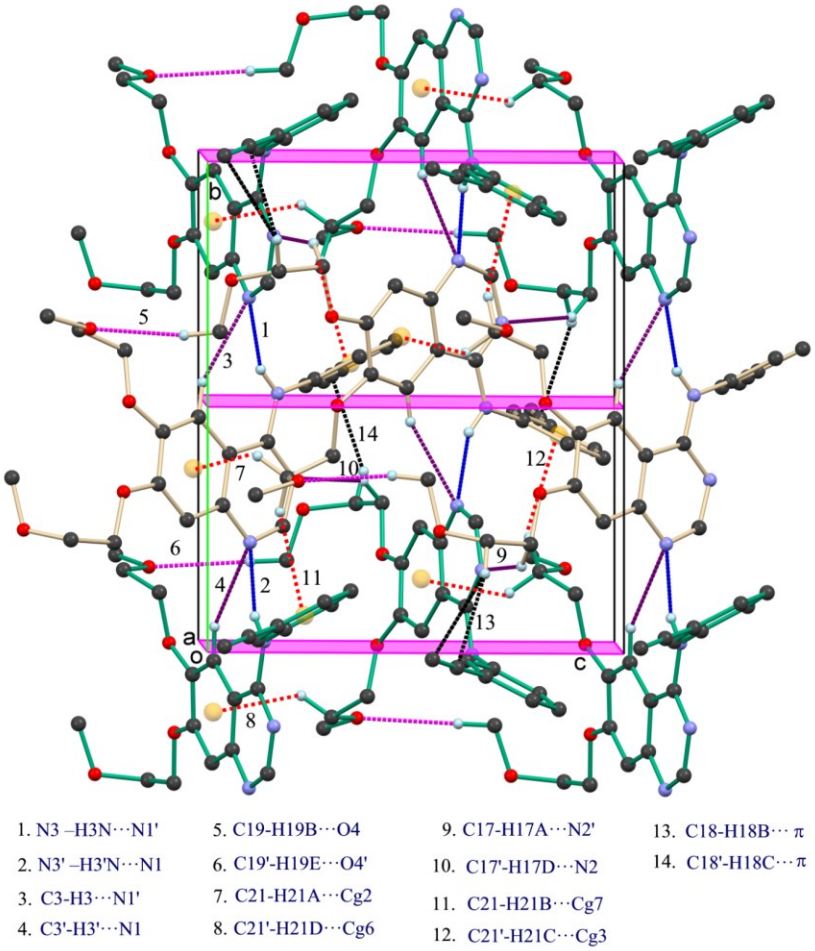

Figure S6. The view of molecular packing down the *a*-axis revealing the compact packing of c-glide symmetry-related molecular chains of symmetry independent molecules using N-H···N (blue), C-H···N (purple), C-H···O (magenta), C-H···π (with phenyl: orange and with C≡C: black) interactions.

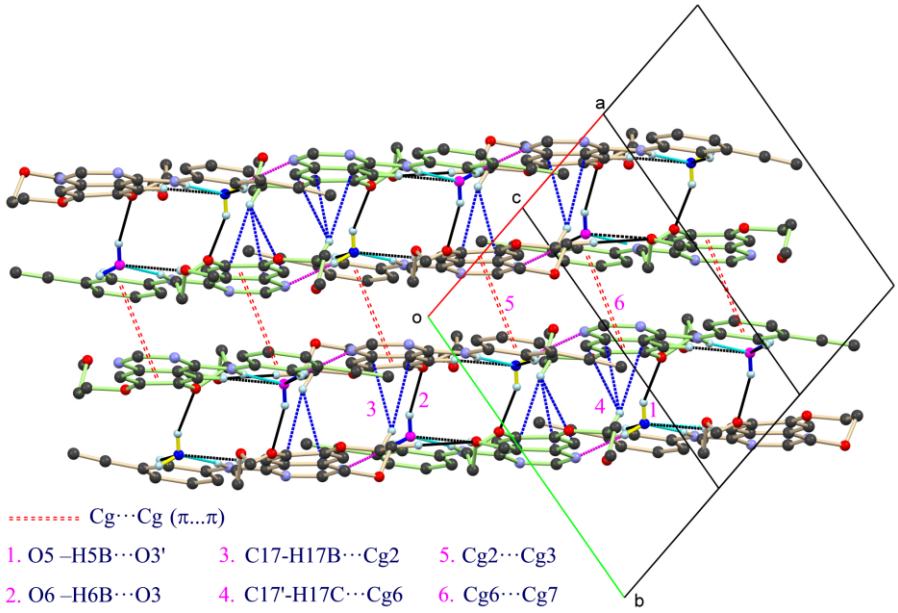

Figure S7. Stitching of the adjacent 2D sheets through O-H···O (methoxy) (black), C-H···π (blue) and π—π (red) stacking interactions.

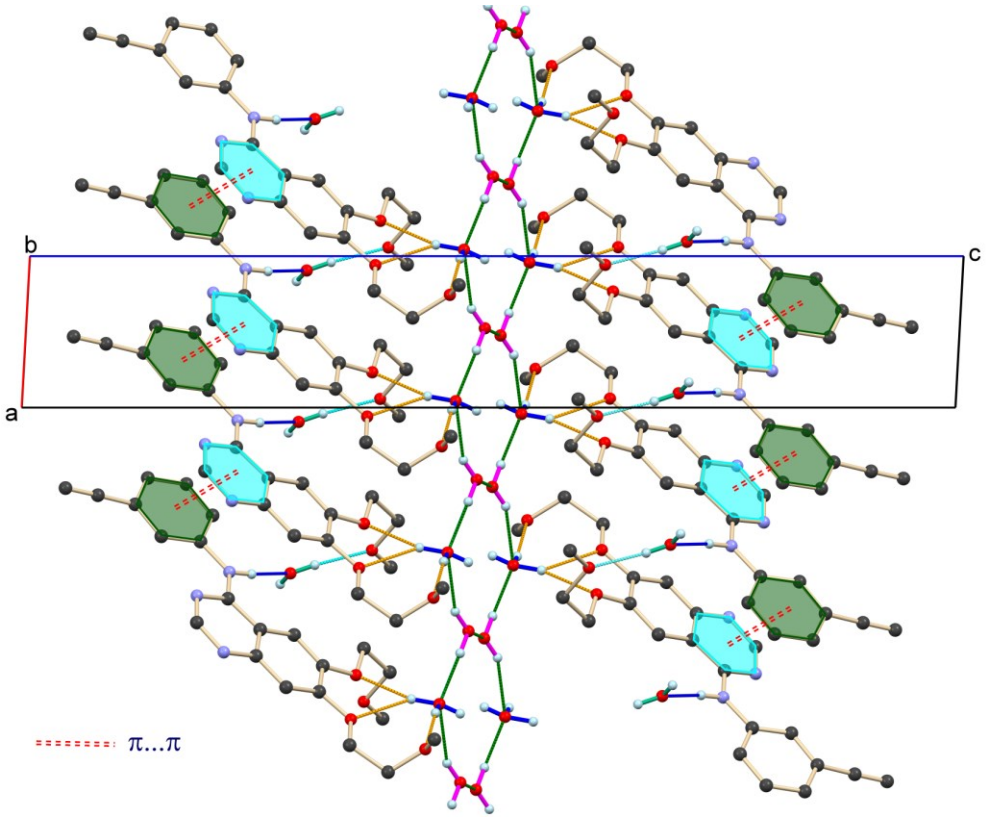

Figure S8. View of molecular packing down b-axis showing water molecules arrangement in the open channel created by ETB molecules along the *c*-axis.

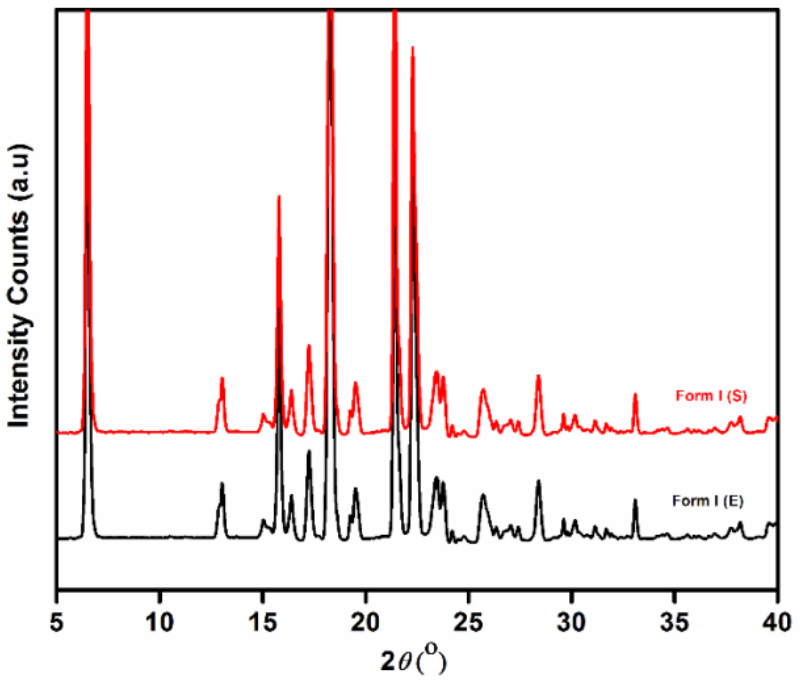
Intensity Counts (a.u)
Form I (S)
Form I (E)
5
10
15
20
25
30
35
40
2θ(°)

(a)

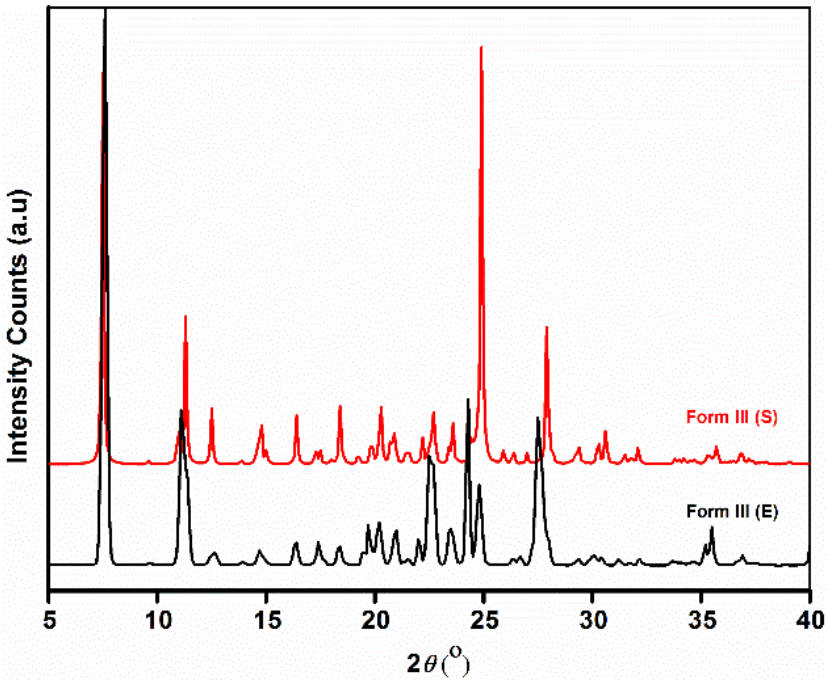
Intensity Counts (a.u)
Form III (S)
Form III (E)
5
10
15
20
25
30
35
40
2θ(°)

(b)

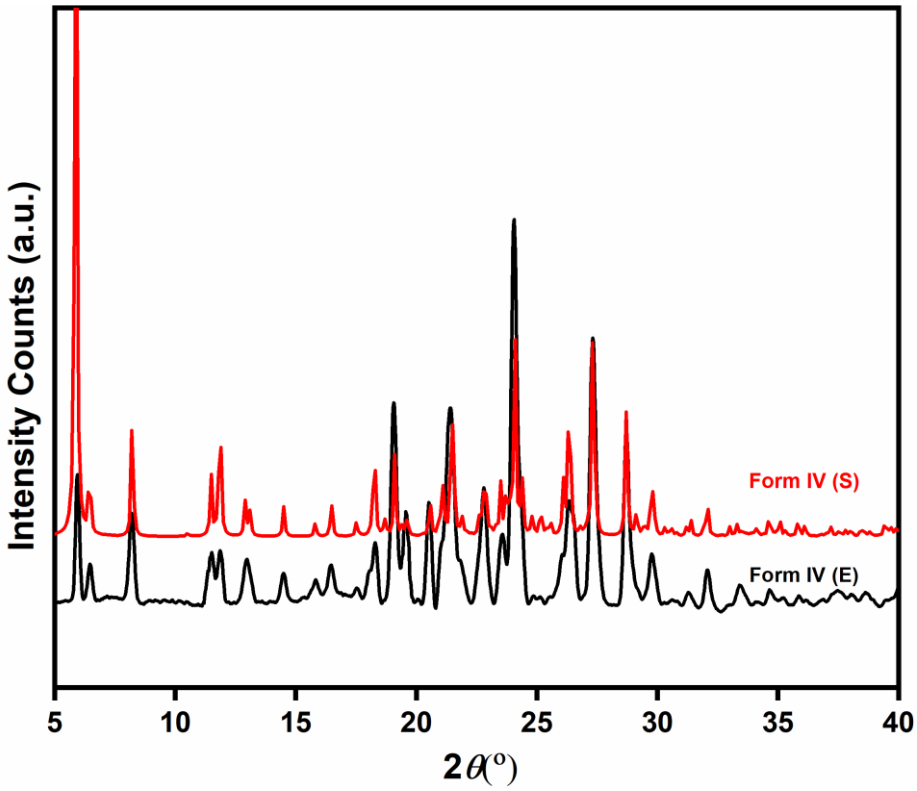

(c)

Figure S9. The overlay of the powder X-ray diffractograms calculated (S) from single-crystal X-ray diffraction data (red) with the experimental (E) data (black) of polymorphs (a) Form I, (b) Form III and (c) Form IV crystals of ETB.

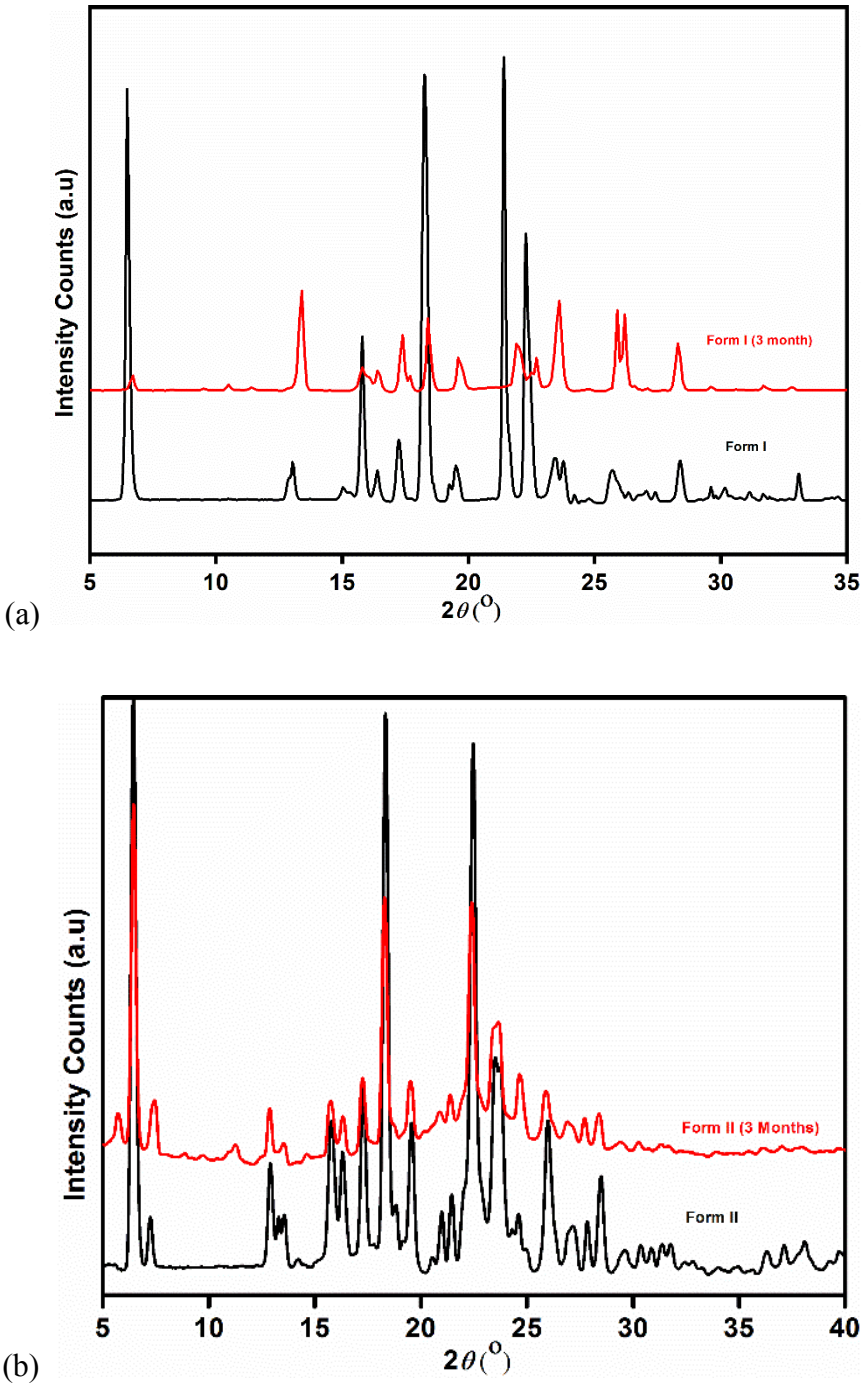

Figure S10. The stacking of the experimental PXRD patterns of erlotinib polymorphs, a) Form I (fresh sample, black) and Form I (after three months, red) and (b) Form II (fresh sample, black) and Form II, (after three months, red).

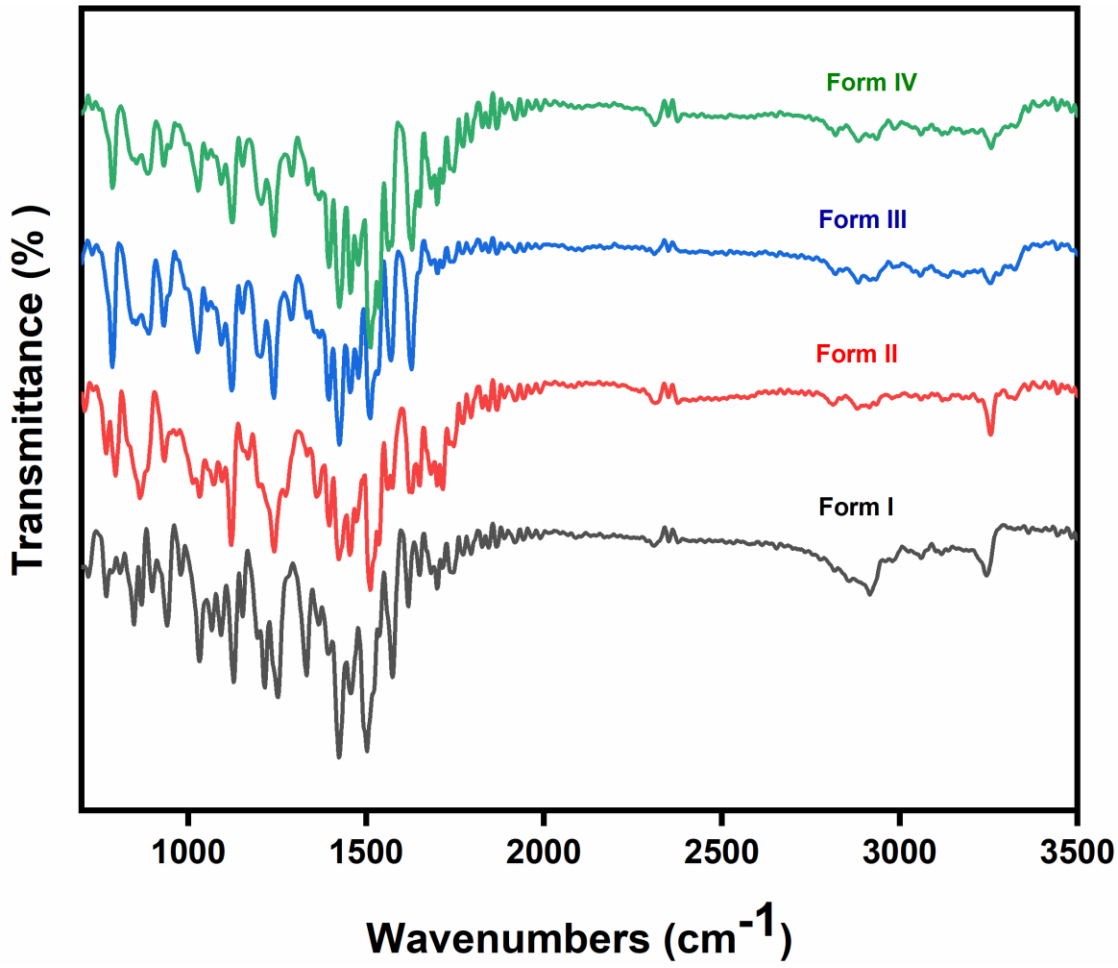

Figure S11. Infra-Red spectra of polymorphs and hydrates of ETB, Form I (black), Form II (red), Form III (blue) and Form IV (green).

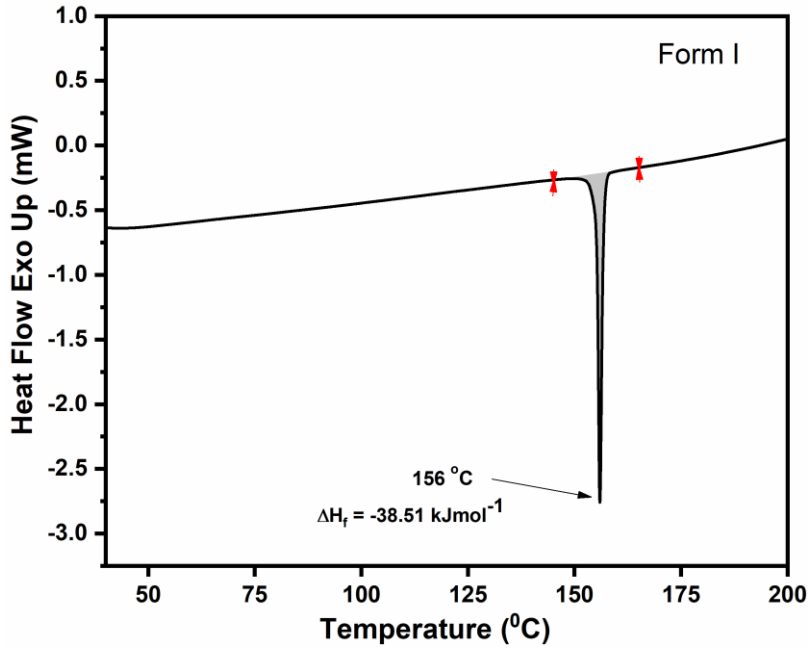
Form I
Heat Flow Exo Up (mW)
1.0
0.5
0.0
-0.5
-1.0
-1.5
-2.0
-2.5
-3.0
156 °C
ΔH_f = -38.51 kJmol^-1
50
75
100
125
150
175
200
Temperature (0C)

(a)

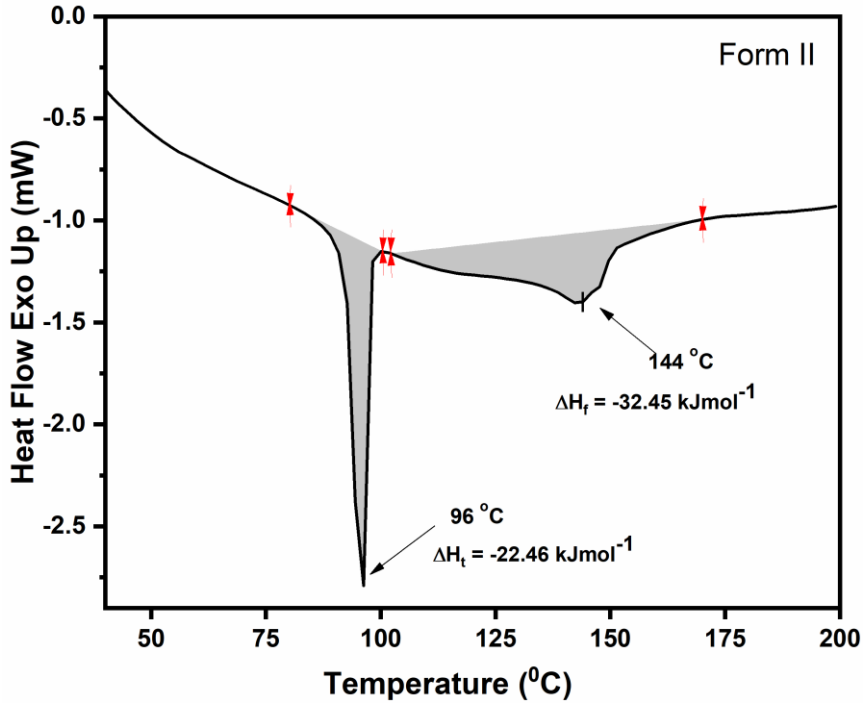
Form II
Heat Flow Exo Up (mW)
0.0
-0.5
-1.0
-1.5
-2.0
-2.5
144 °C
ΔH_f = -32.45 kJmol^-1
96 °C
ΔH_t = -22.46 kJmol^-1
50
75
100
125
150
175
200
Temperature (0C)

(b)

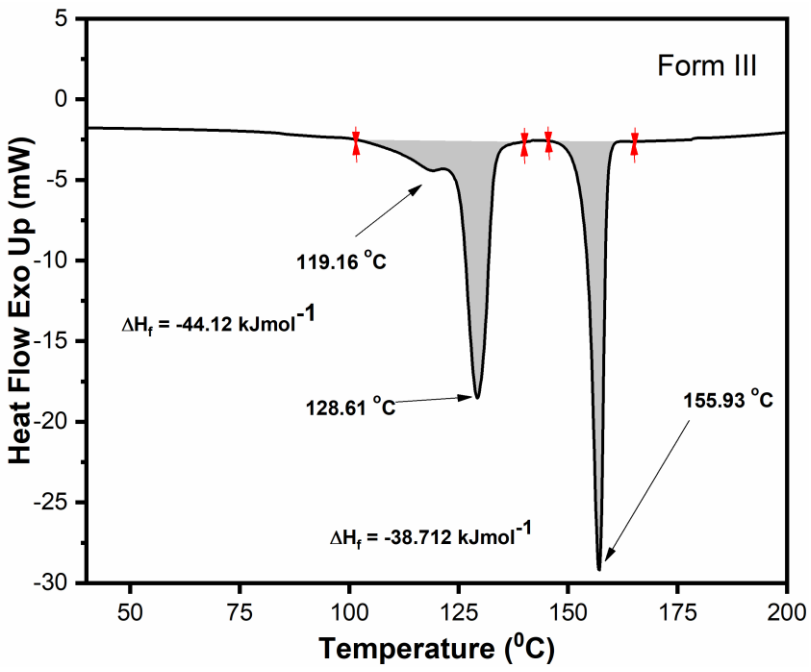

(c)

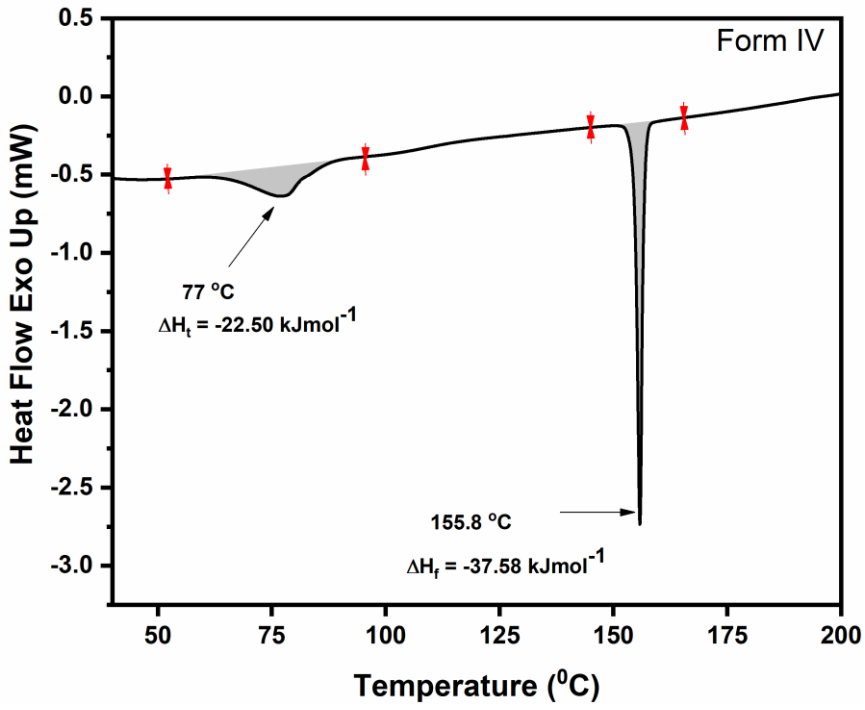

(d)

Figure S12. DSC thermograms of ETB solid phases, (a) Form I, (b) Form II, (c) Form III (monohydrate) and (d) Form IV (trihydrate).

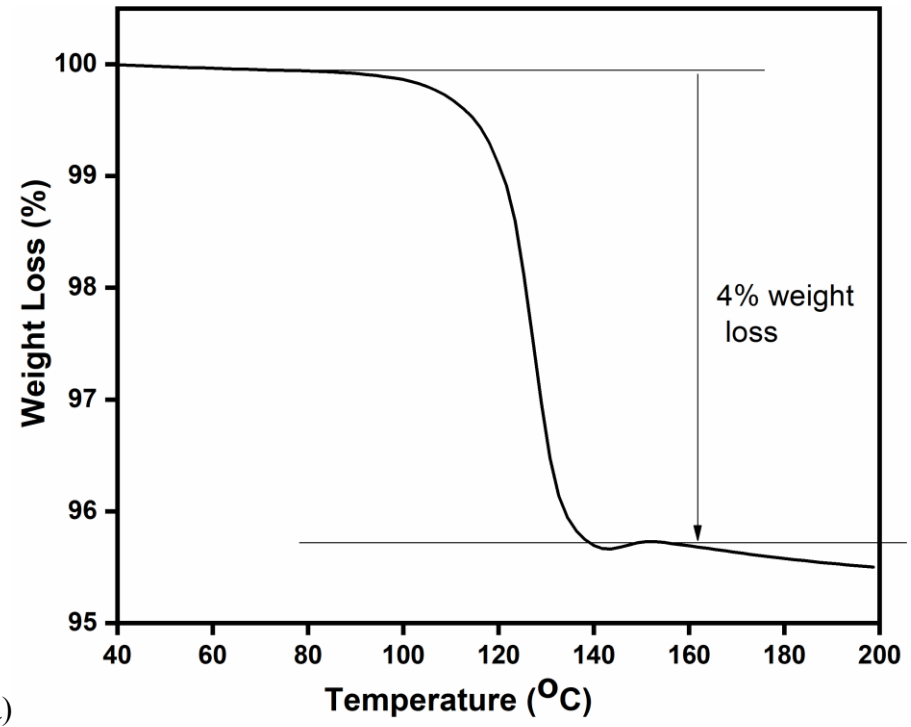

(a)

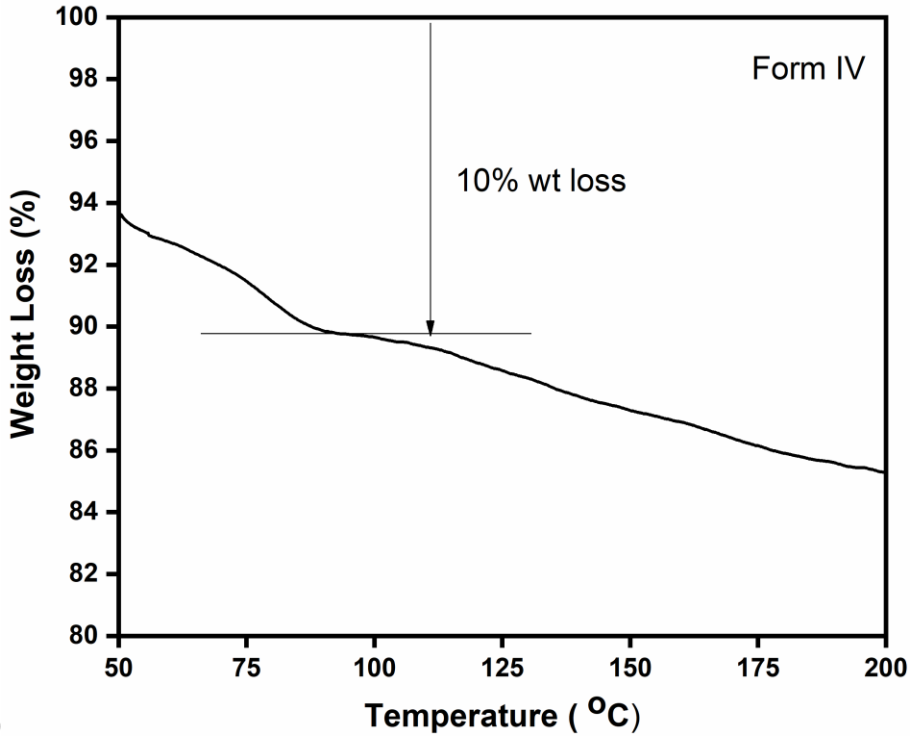

(b)

Figure S13. The TGA thermograms of hydrates of ETB, (a) Form III and (b) Form IV.

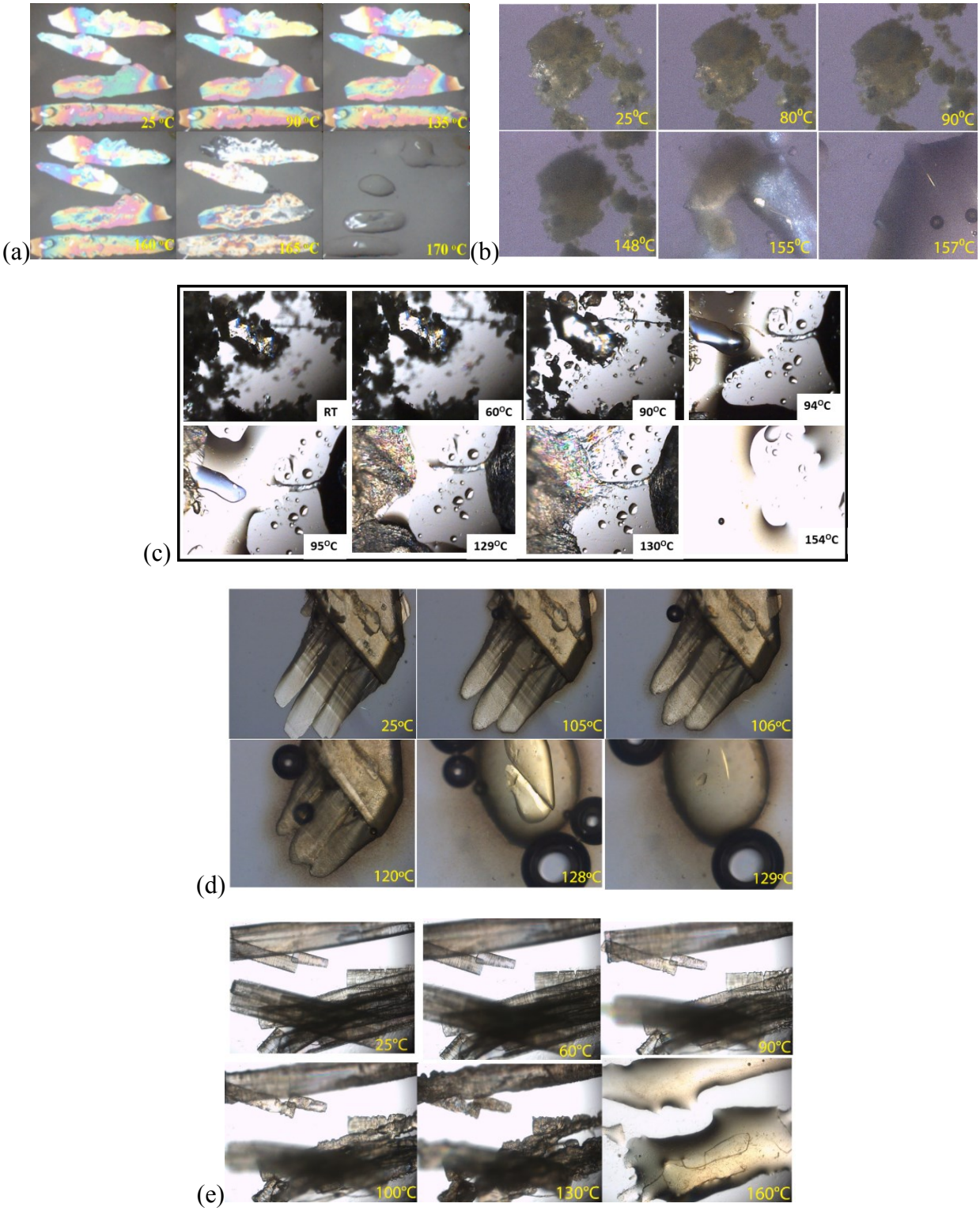

Figure S14. The photomicrographs of the ETB polymorphs during the HSM study, (a) Form I, (b) From II, (c) Form III (in paraffin oil), (d) Form III (without oil), and (e) From IV.

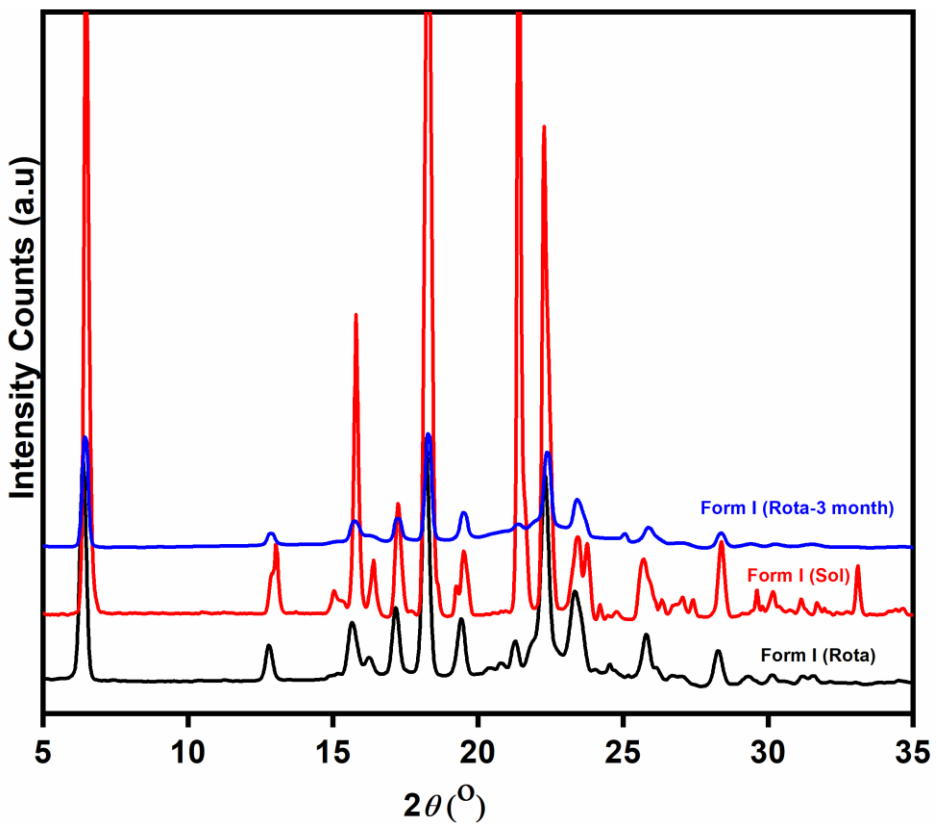

Figure S15. The overlay of the experimental PXRD patterns of ETB Form I crystals, obtained by solution crystallization (red), polycrystalline material obtained by fast crystallization over a rotary evaporator (black) and same polycrystalline sample after three months (blue).

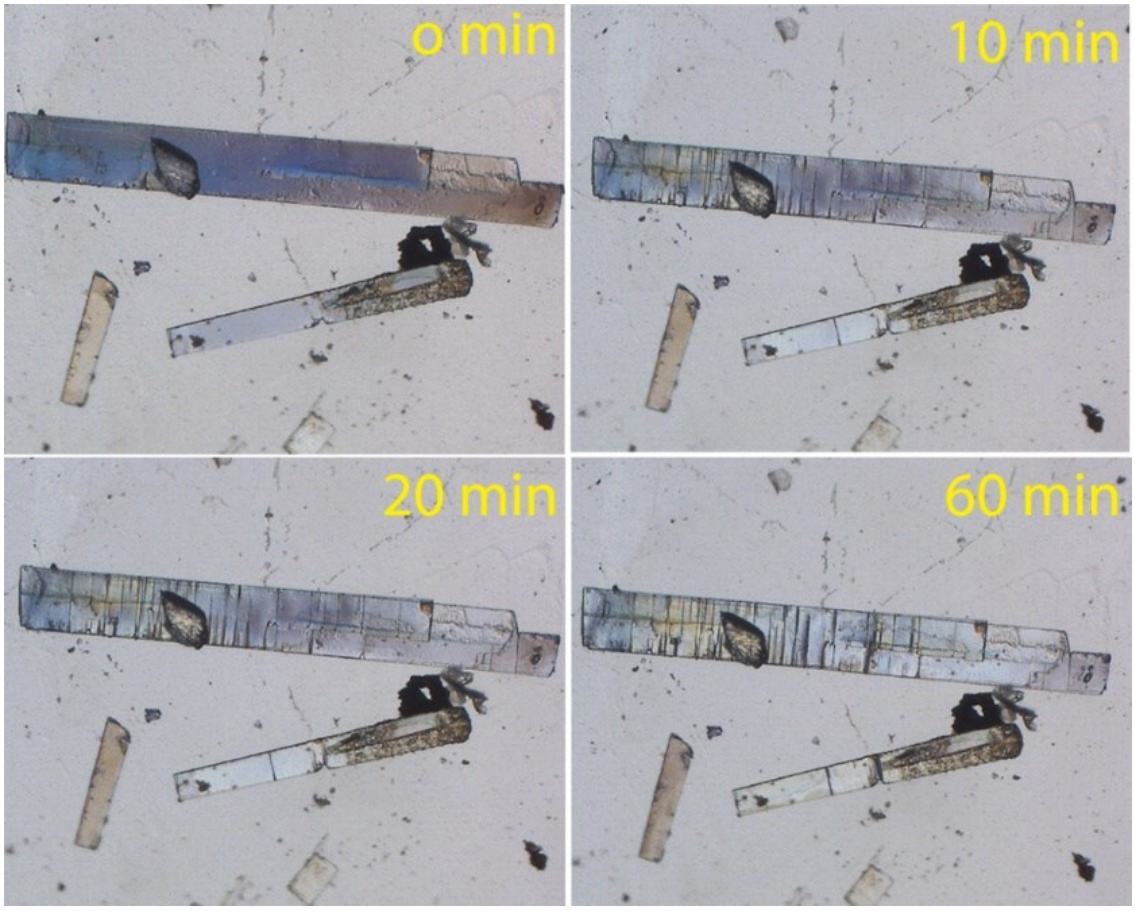

Figure S16. The photomicrographs of the Form IV crystals taken at ambient conditions at different time interval.

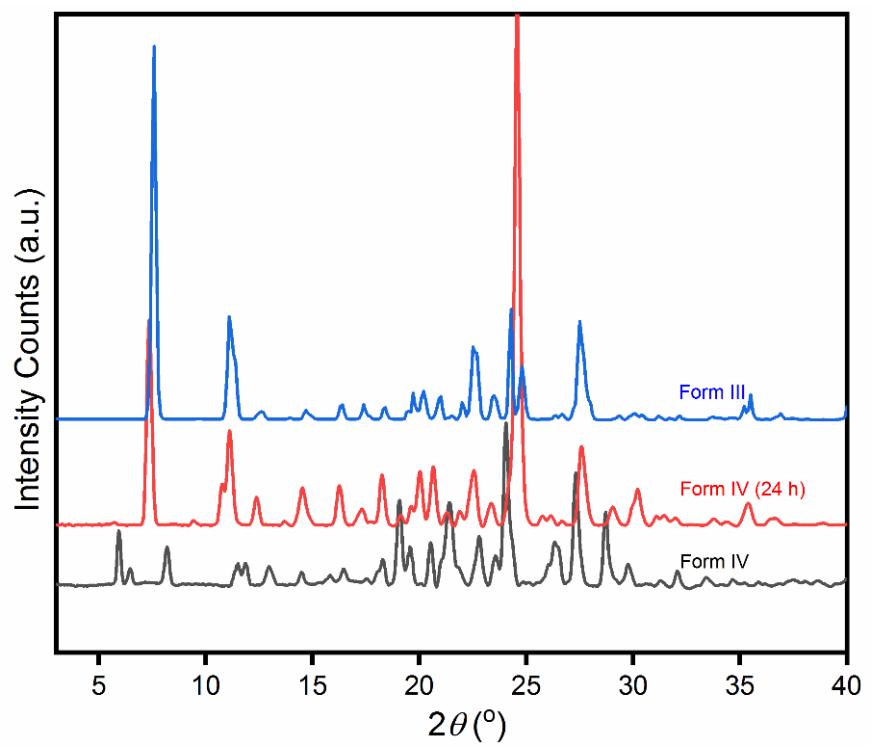

Figure S17. The PXRD profiles showing the conversion of Form IV (black) to Form III (red) after 24 H (red).

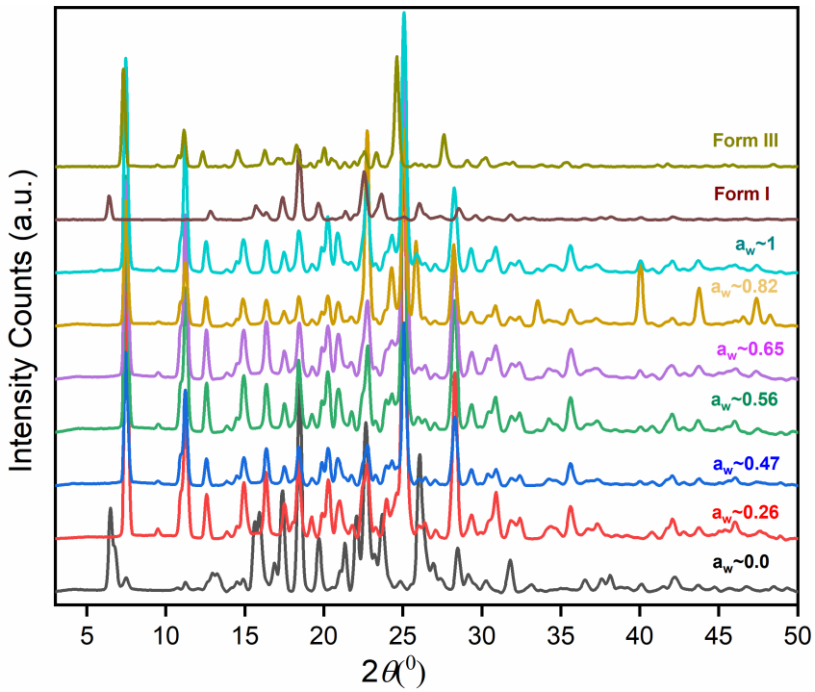

Figure S18. PXRD profiles of the residual samples at equilibrium after 3 days of continuous stirring in competitive slurry experiment with varying water activity.

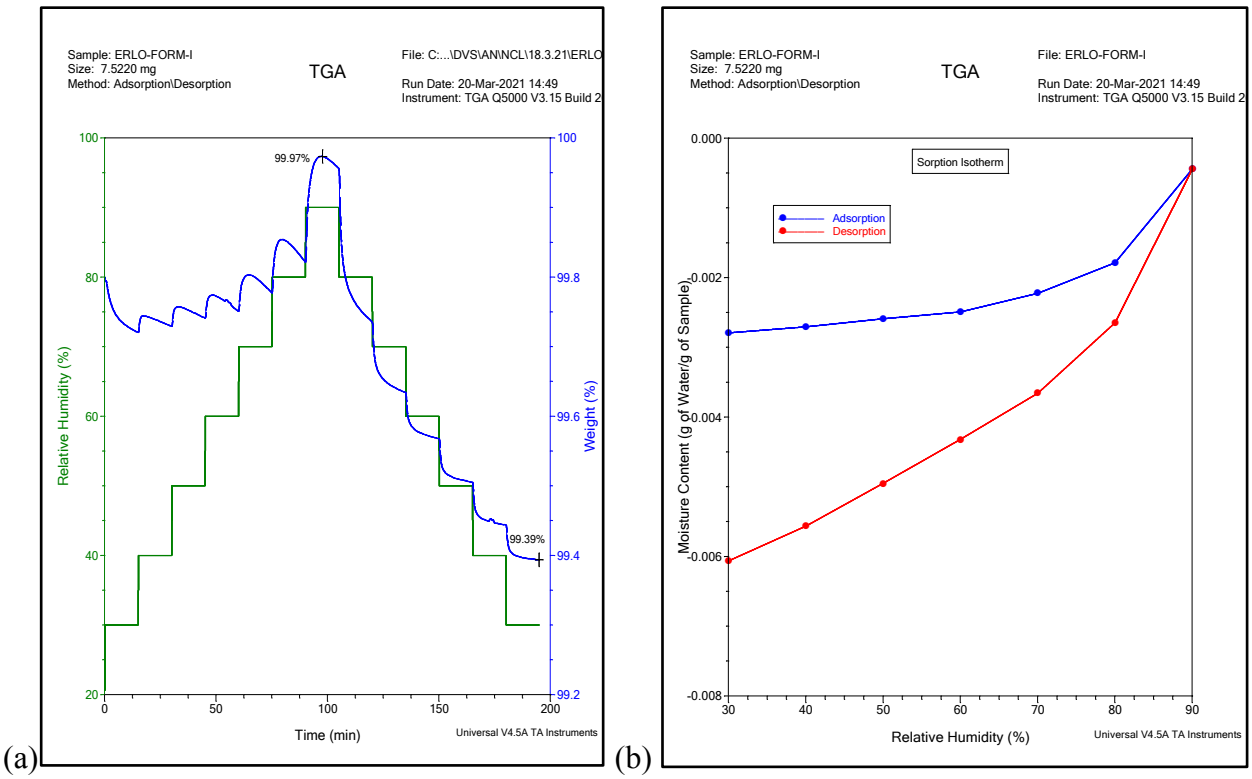

Figure S19. (a) Dynamic vapor sorption profile for Form I of ETB recorded over a relative humidity range of 30–90% RH with a step size of 10% RH at 40 °C and (b) the corresponding sorption isotherm.

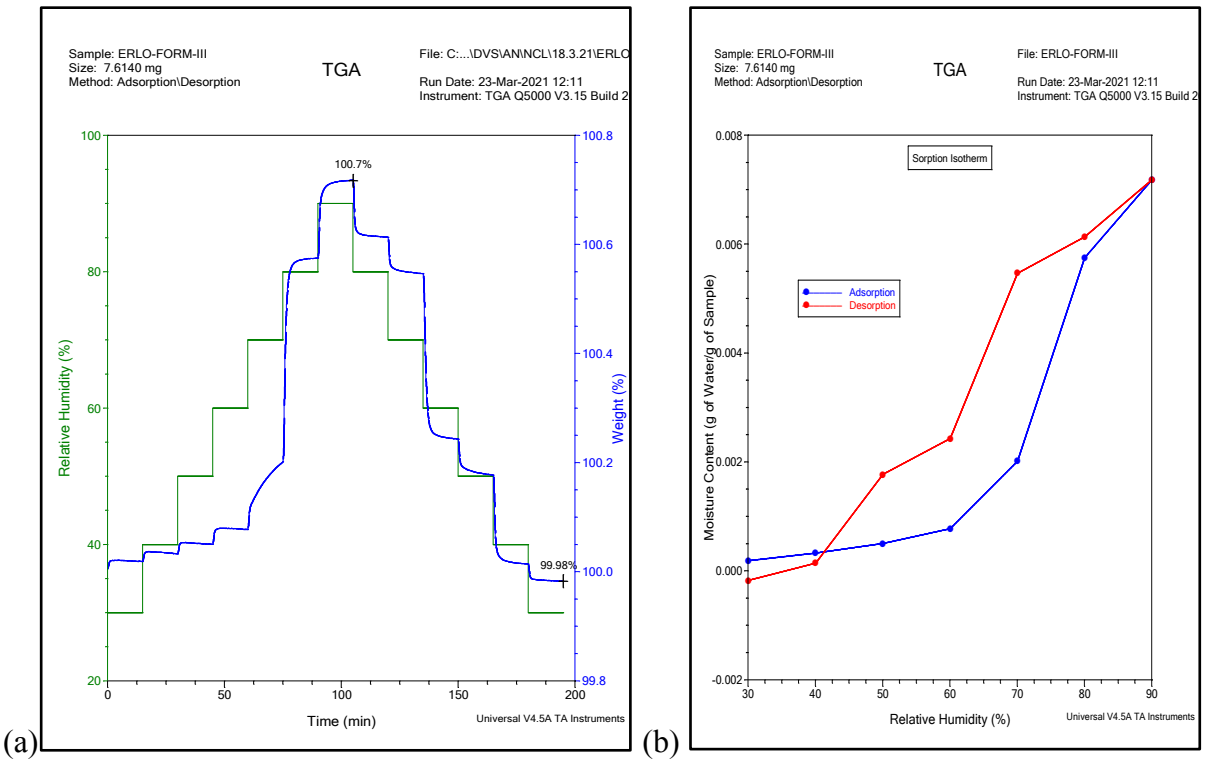

Figure S20. (a) Dynamic vapor sorption profile for Form III of ETB recorded over a relative humidity range of 30–90% RH with a step size of 10% RH at 40 °C and (b) the corresponding sorption isotherm.

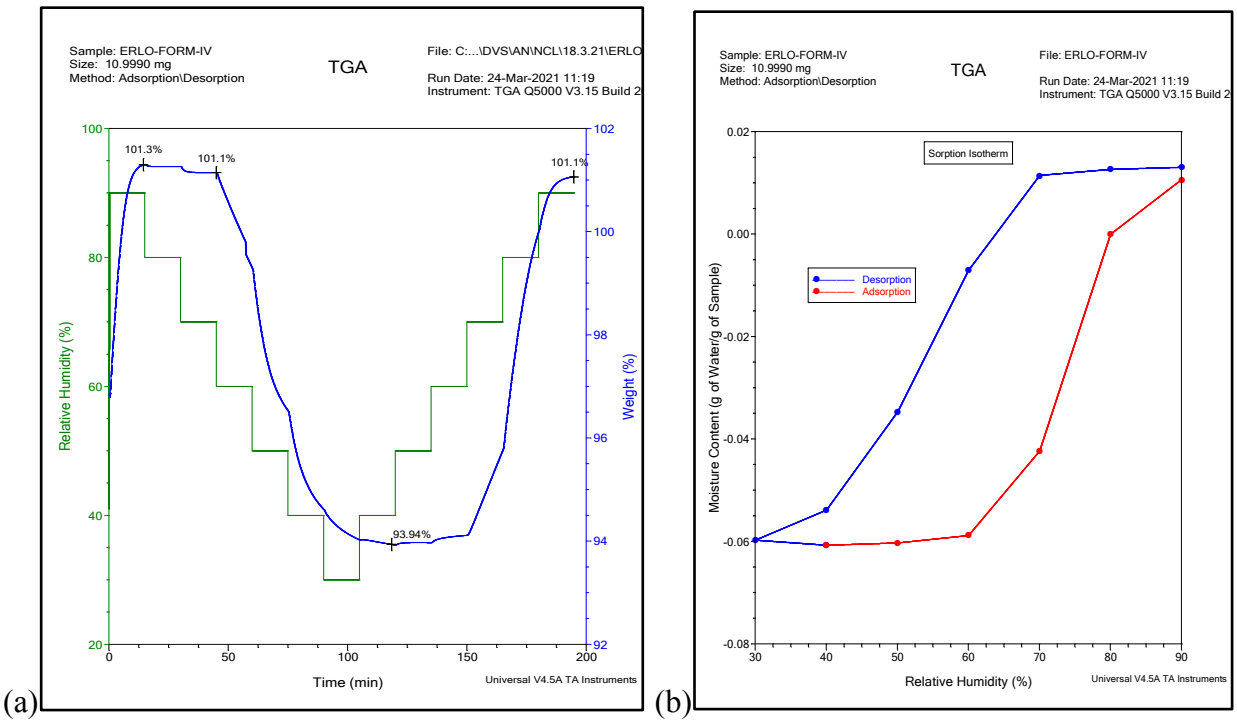

Figure S21. (a) Dynamic vapor sorption profile for Form IV of ETB recorded over a relative humidity range of 30–90% RH with a step size of 10% RH at 40 °C and (b) the corresponding sorption isotherm.

(a)

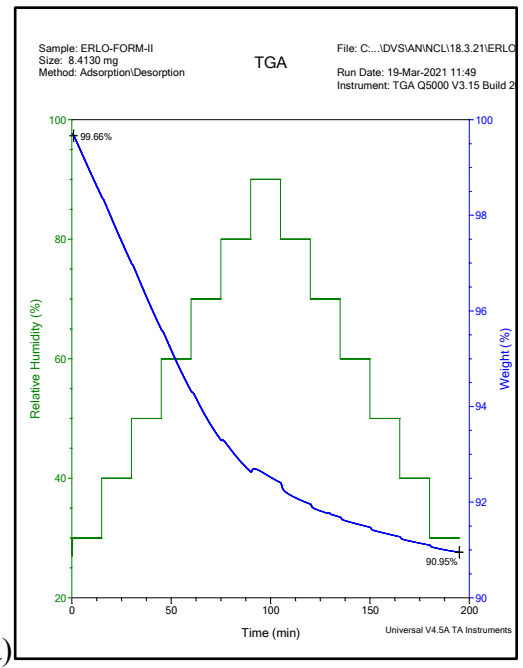

(b)

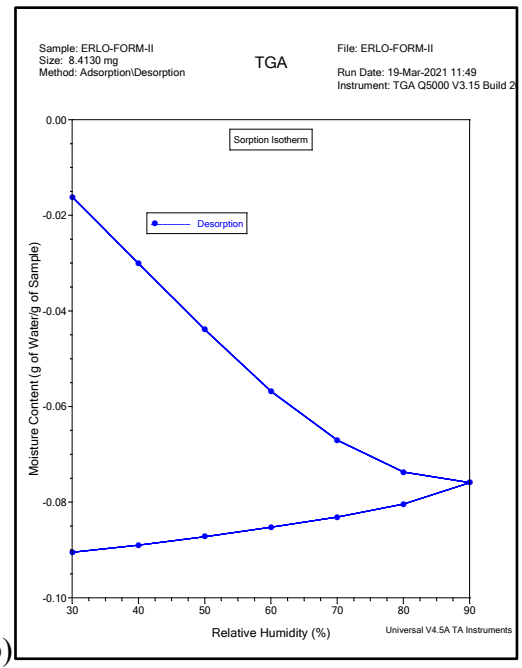

Figure S22. (a) Dynamic vapor sorption profile for Form II of ETB recorded over a relative humidity range of 30–90% RH with a step size of 10% RH at 40 °C and (b) the corresponding sorption isotherm.

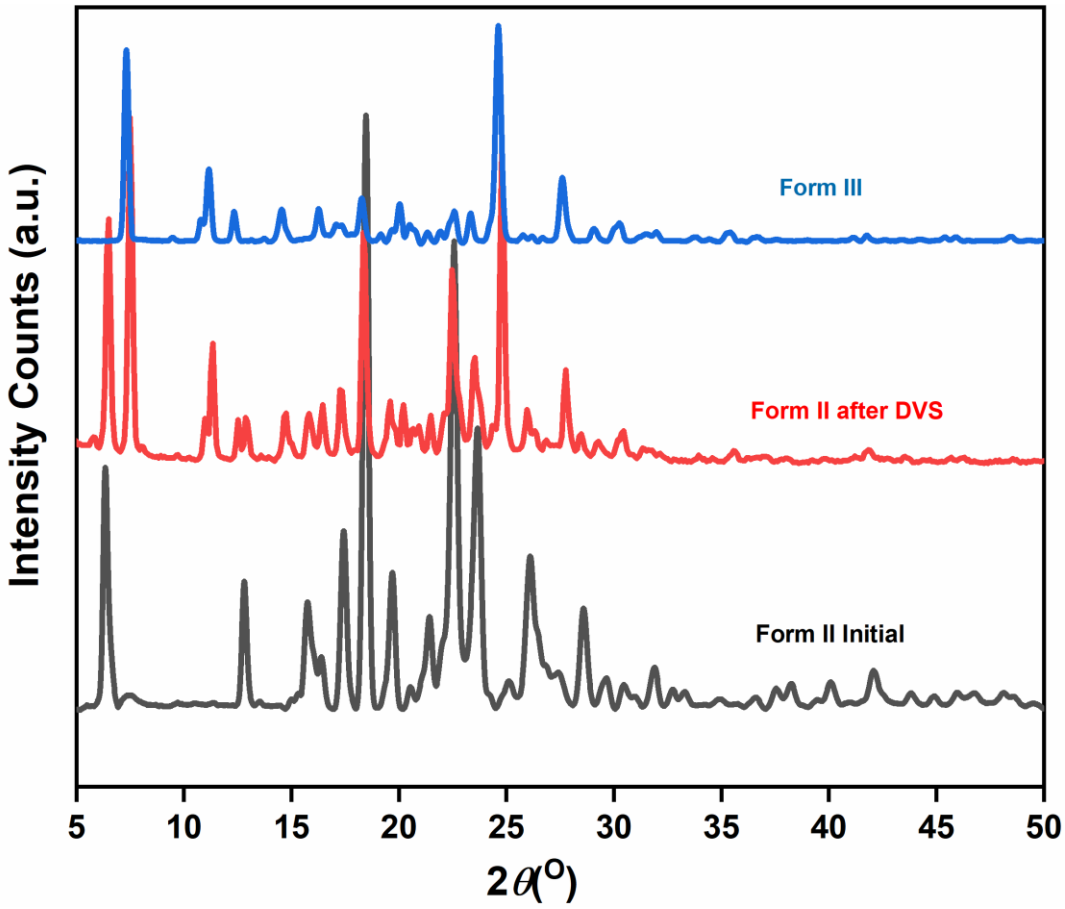

Figure S23. Overlay of the PXRD pattern of Form II recorded after DVS studies with PXRD profiles of Form II and Form III.

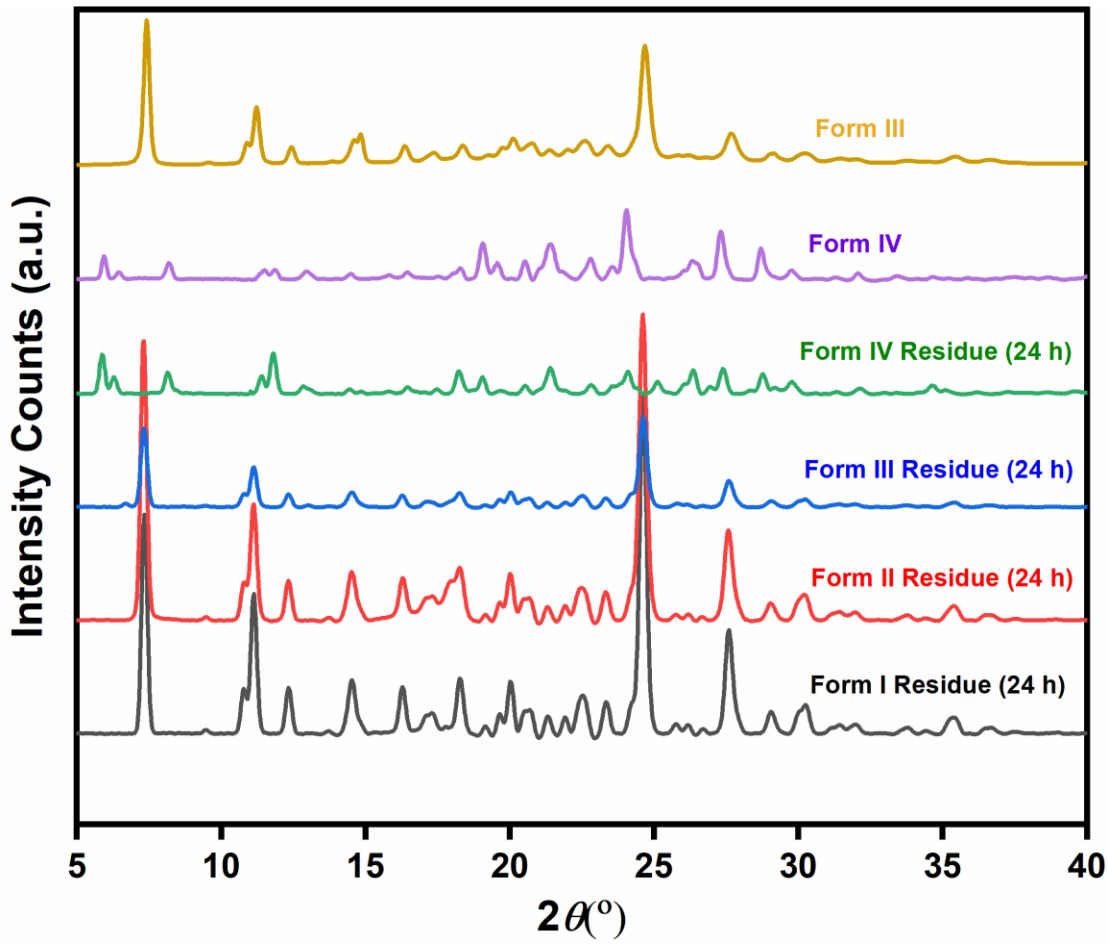

Figure S24. PXRD overlay of the residual samples after solubility study in Millipore water after 24 h.

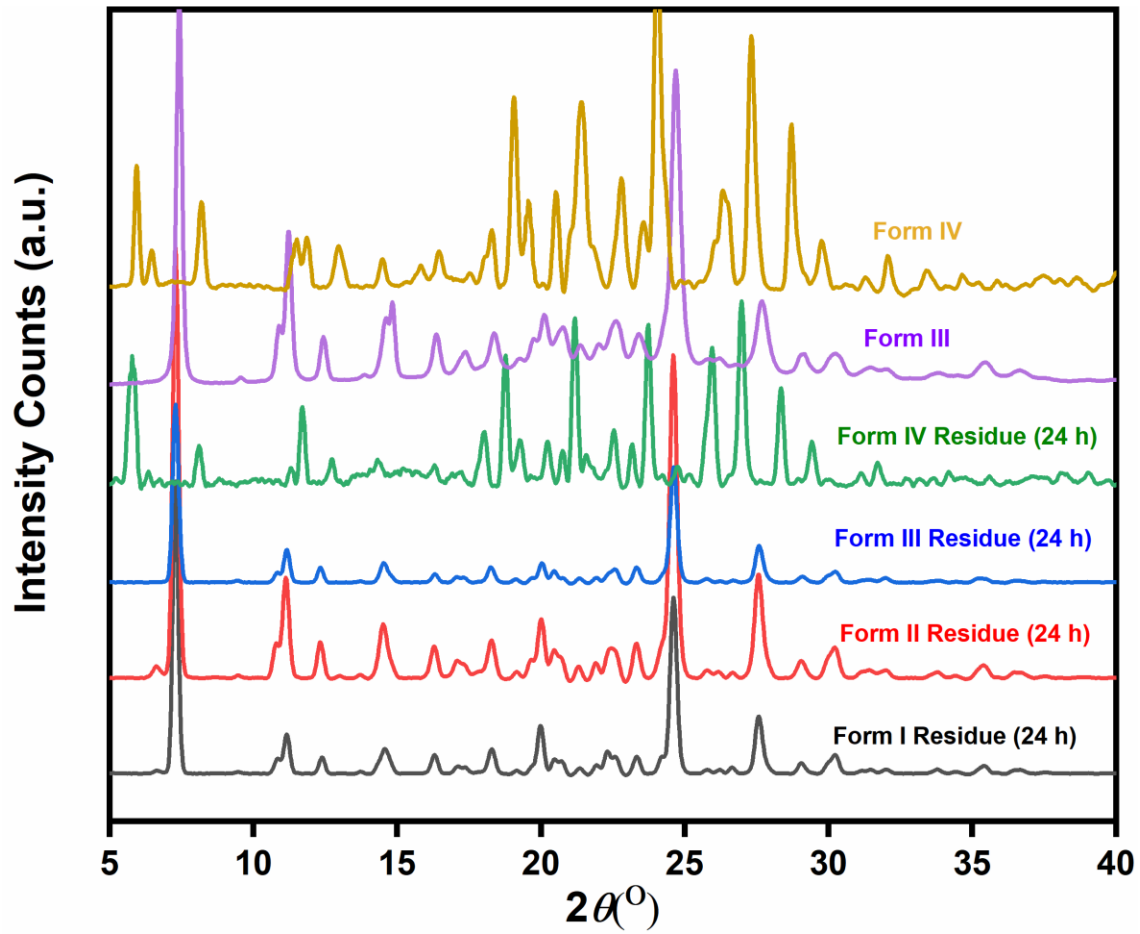

Figure S25. PXRD overlay of the residual samples after solubility study in pH 3 HCL solution after 24 h.

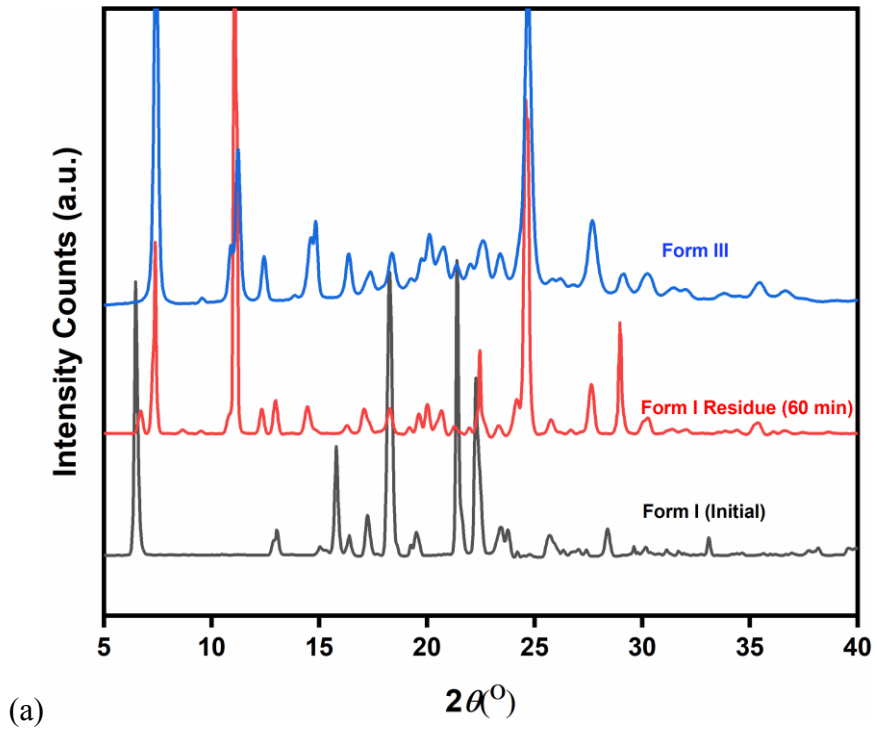

(a)

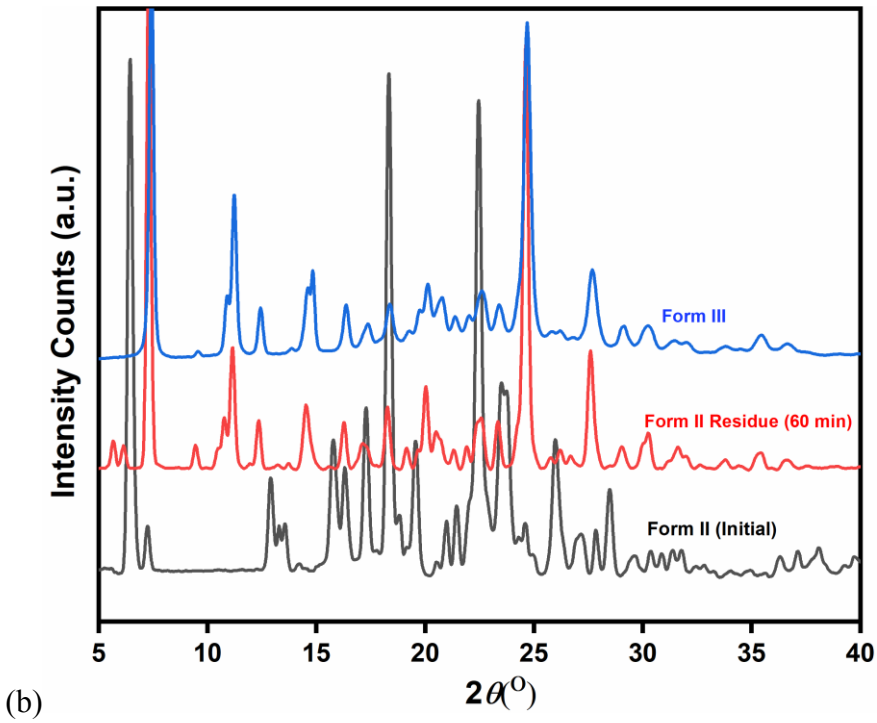

(b)

Figure S26. PXRD overlay of the residual samples of (a) Form I and (b) Form II after dissolution rate measurement in 3 pH HCL solution for 60 minutes.

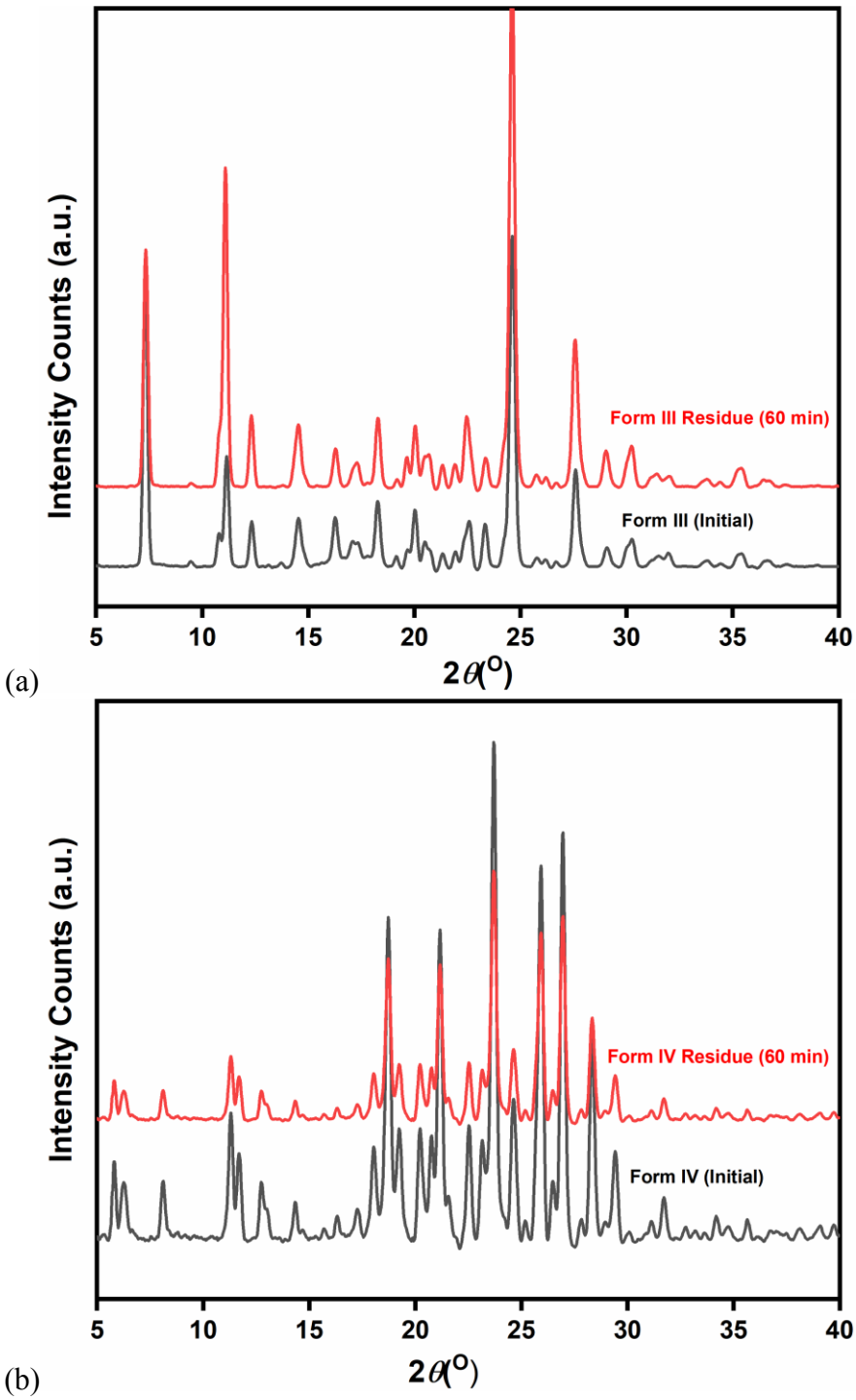

Figure S27. PXRD overlay of the residual samples of (a) Form III and (b) Form IV after dissolution rate measurement in 3 pH HCL solution for 60 minutes.

Table S1. Crystal data of Form III of ETB collected at 150(2) K.

	ETB-Form III at 150 (K)
Chem. Formula	$C_{22}H_{23}N_3O_4 \cdot H_2O$
Formula weight	411.45
Temperture (K)	150(2)
Crystal size	0.42 x 0.38 x 0.32
Crystal system	triclinic
Space group	*P*-1
a/Å	8.9682(14)
b/Å	10.4171(16)
c/Å	13.070(2)
α/°	98.475(2)
β/°	108.766(2)
γ/°	111.776(2)
V/Å^3	1023.0(3)
Z, D_{calc} g/cm^3	2, 1.336
μ/mm^{-1}	0.096
F (000)	436
θ max/°	25.0
Absorption correction	multi-scan
Reflections collected	10350
Unique reflections	3597
Observed reflections	2816
R_{int}, R_{sig}	0.0335, 0.0332
h, k, l (min, max)	(-10, 10), (-12, 12), (-15, 15)
parameters/restraints	293/4
R_1_obs, R_1 _*all*	0.0612, 0.0801
wR_2_obs, wR_2_*all*	0.1382, 0.1478
Goodness-of-fit on F^2	1.061
$\Delta\rho_{max}$, $\Delta\rho_{min}$ (eÅ^{-3})	0.388, -0.223

Table S2. Torsion angle (°) for polymorphs of erlotinib

polymorphs	Torsion angle	Torsion Angle Values (°)
Form I	C17-C18-O2-C19	89.06(18)
	C17'-C18'-O2'-C19'	-86.4(2)
	C20-C21-O4-C22	171.96(13)
	C20'-C21'-O4'-C22'	-169.32(14)
Form III	C17-C18-O2-C19	92.33(6)
	C17'-C18'-O2'-C19'	174.67(6)
	C20-C21-O4-C22	166.64(5)
	C20'-C21'-O4'-C22'	137.79(7)
Form IV	C17-C18-O2-C19	80.26(19)
	C20-C21-O4-C22	165.87(13)

Table S3. The geometrical parameters of intermolecular interactions of ETB solid phases.

	D-H···A	D-H (Å)	H···A (Å)	D···A/ Cg···Cg (Å)	D-H···A /α (o)
Form I	N3-H3N···N1'	0.88	2.08	2.913(2)	157
	N3'-H3'N···N1^{i}	0.88	2.08	2.903(2)	155
	C3-H3···N1'	0.95	2.62	3.524(2)	158
	C3'-H3'···N1^{i}	0.95	2.66	3.558(2)	158
	C16-H16···O4^{ii}	0.95	2.61	3.274(2)	127
	C16'-H16'···O4'^{iii}	0.95	2.53	3.032(2)	113
	C19-H19B···O4^{iv}	0.98	2.57	3.535(2)	170
	C19'-H19E···O4'^{v}	0.98	2.70	3.679(2)	176
	C21-H21A…Cg2^{iv}	0.99	2.85	3.479(2)	122
	C21'-H21D…Cg6^{v}	0.99	2.74	3.408(2)	125
	C21-H21B…Cg7^{v}	0.99	2.85	3.673(2)	141
	C21'-H21C…Cg3^{v}	0.99	2.84	3.656(2)	141
	C17-H17A···N2'^{iv}	0.99	2.48	3.348(2)	146
	C17'-H17D···N2^{iv}	0.99	2.53	3.383(2)	145
	C18-H18B…πi^{v}	0.99	2.64	3.546(2)	152
	C18'-H18C…πi^{v}	0.99	2.77	3.633(2)	146
Form III	N3-H3N···O5	0.88(1)	2.16(1)	3.022(1)	166.5(10)
	C3-H3···O5	0.95	2.27	3.208(1)	169
	C14-H14···O5	0.95	2.48	3.301(1)	144
	N3'-H3'N···O6	0.88(1)	2.20(1)	3.066(1)	166.6(10)
	C3'-H3'···O6	0.95	2.24	3.189(1)	173
	C14' –H14'···O10	0.95	2.45	3.284(1)	146
	O5–H5A···N1'^{i}	0.86(1)	2.00(1)	2.855(1)	174.2(12)
	O6 –H6A···N1^{ii}	0.87(1)	1.97(1)	2.843(1)	175.0(12)
	C18 –H18B···O4'^{ii}	0.99	2.67	3.487(2)	140
	O5 –H5B···O3'	0.86(1)	2.18(1)	2.976(1)	154.9(12)
	O6 –H6B···O3	0.85(1)	2.27(1)	3.036(1)	158.6(12)

	C17-H17B···Cg2[ii]	0.99	2.67	3.536(1)	147
	C17'-H17C···Cg6[i]	0.99	2.61	3.511(1)	152
	Cg2··· Cg3[iii]			3.651(1)	9.31(2)
	Cg6···Cg7iv			3.689(1)	5.04(2)
Form IV	N3-H3N···O5	0.88	2.11	2.959(1)	161
	C3-H3···O5	0.95	2.30	3.240(1)	168
	C10-H10···O5	0.95	2.43	3.217(1)	140
	C20-H20B···O5	0.99	2.66	3.490(2)	142
	O6-H6A···O1	0.92(2)	2.39(2)	3.131(1)	137(2)
	O6-H6A···O3	0.92(2)	2.13(2)	2.983(1)	154(2)
	O6-H6B···O2	0.88(2)	2.07(2)	2.931(1)	165(3)
	O8-H8B···O6	0.82(2)	1.95(2)	2.720(3)	157(3)
	O7-H7A···O6[i]	0.84(10)	2.23(10)	3.008(3)	156(12)
	O7-H7B···O8[ii]	1.08	1.70	2.769(4)	174
	O5-H5B···N1[iii]	0.84(2)	1.96(2)	2.793(1)	170.6(14)
	O5-H5A···O4[i]	0.86(2)	1.98(2)	2.832(1)	175.7(14)
	C1-H1···O4[iv]	0.95	2.63	3.451(2)	145
	Cg1···Cg3[v]			3.746(2)	10.45(5)

D-H = Donor- Hydrogen bond length in Angstrom (Å), H···A = Hydrogen···Acceptor bond length in Angstroms (Å), D···A = Donor···Acceptor bond length in Angstroms (Å), D-H···A = bond angle in degrees (°), Cg = Center of gravity of ring, C-H···Cg = distance between H and Cg, Cg···Cg = distance between ring centroids in Angstroms (Å), α = dihedral angle between planes of two aromatic rings in degrees (°), Cg1 = N1/C1/N2/C2/C8/C7, Cg2 = C3-C8, Cg3 = C9-C14, Cg6 = C3'-C8', Cg7 = C9'-C14'.

Symmetry Codes for Form I: (i) *x*, *y*-1, *z*; (ii) *x*+1, -*y*+1, *z*+1/2; (iii) *x*-1, *y*, *z*; (iv) *x*, -*y*+1, *z*-1/2; (v) *x*, -*y*, *z*-1/2; Symmetry Codes for Form III: (i) -*x*+1,-*y*+1,-*z*+1; (ii) -*x*, -*y*, -*z*; (iii) -*x*+1, -*y*, -*z*; (iv) -*x*,-*y*+1,-*z*+1; Symmetry Codes for Form IV: (i) *x*-1, *y*, *z*; (ii) -*x*+1,-*y*+1,-*z*+1; (iii) -*x*+1, *y*+1/2, -*z*+1/2; (iv) –*x*+1, *y*-1/2, -*z*+1/2; (v) *x*+1, *y*, *z*.

Table S4. ETB solid phases in competitive Slurry experiment

Methanol (Mole Fraction	**Water (Mole Fraction)**	**Water Activity (a_w)**	**ETB Phase**
1	0	0	Form I, III
0.8	0.2	0.2606792	Form III
0.6	0.4	0.4732352	Form III
0.5	0.5	0.56725625	Form III
0.4	0.6	0.6554792	Form III
0.2	0.8	0.8228672	Form III
0	1	1	Form III

Water activity values in methanol-water mixture were calculated using the mathematical expression,

$a_w = 0.0056 + 1.398x_w - 0.647x_w^2 + 0.153x_w^3 + 0.845x_w^4$

wherein,

a_w – water activity

x_w – mole fraction of water

(Reference: Influence of water activity in organic solvent + water mixtures on the nature of the crystallizing drug phase. 1. Theophylline. H. Zhu, C. Yuen and D. J. W. Grant, *Int. J. Pharm.*, 1996, **135**, 151-160.)

Table S5. Equilibrium solubility in Millipore water and pH 3 HCl solution

	Millipore water (pH 6.9) (μg/mL)	**pH 3 HCl Solution (μg/mL)**
Form I	3.34±0.25	283.67±0.58
Form II	1.79±0.24	291.67±3.51
Form III	2.01±0.13	293.67±11.02
Form IV	1.88±0.07	227.67±15.28
ETB-HCl	185.11±3.67	335.33±10.07

Table S6. Dissolution rate measurement in pH 3 HCl solution

Time (min)	ETB-HCl (μg/mL)	Form I (μg/mL)	Form I (Polycrystalline) (μg/mL)	Form II (μg/mL)	Form III (μg/mL)	Form IV (μg/mL)
0	0±0	0±0	0±0	0±0	0±0	0±0
5	102.56±2.51	56.33±2.66	82.1±2.01	129.66±6.12	6.76±0.17	28.27±0.69
10	166.42±4.08	78.51±2.01	89.68±2.2	141.88±3.63	7.5±0.18	30.1±0.74
15	209.24±5.13	84.37±4.68	95.86±2.35	150.43±8.35	9.15±0.22	40.55±0.99
20	239.34±8.36	90.86±2.23	104.34±3.65	161.82±3.96	10.93±0.38	42.99±1.5
25	267.07±6.54	91.39±2.24	113.8±2.79	174.89±4.28	13.26±0.32	47.3±1.16
30	278.59±5.48	93.85±5.31	119.1±2.34	188.86±10.69	13.06±0.26	53.06±1.04
35	302.54±7.41	92.38±3.82	126.93±3.11	183.36±7.57	15.09±0.37	56.36±1.38
40	325.94±9.66	94.93±2.33	131.06±3.88	196.36±4.81	16.76±0.5	62.88±1.86
45	324.07±7.94	100.66±1.98	135.13±3.31	196.97±3.87	17.96±0.44	63.01±1.54
50	342.09±8.73	101.99±3.62	138.6±3.54	201.25±7.15	20.75±0.53	69.42±1.77
55	356.92±8.74	103.26±2.53	142.55±3.49	209.36±5.13	21.53±0.53	68.58±1.68
60	370.64±7.41	105.12±5.93	151.2±3.02	213.43±12.05	23.36±0.47	70.5±1.41